Lab on a Chip

Highly flexible and compact magnetoresistive analytic devices

Journal:	*Lab on a Chip*
Manuscript ID:	LC-ART-06-2014-000751.R1
Article Type:	Paper
Date Submitted by the Author:	01-Aug-2014
Complete List of Authors:	Lin, Gungun; IFW Dresden, Institute for Integrative Nanosciences Makarov, Denys; IFW Dresden, Institute for Integrative Nanoscience Melzer, Michael; IFW Dresden, Institute for Integrative Nanoscience Si, Wenping; IFW Dresden, Institute for Integrative Nanosciences Yan, Chenglin; IFW Dresden, Institute for Integrative Nanoscience; Soochow University, School of Energy Schmidt, Oliver; IFW Dresden, Institute for Integrative Nanosciences

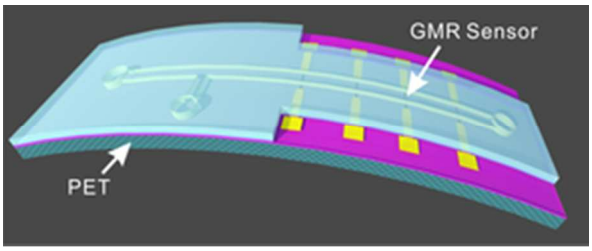

Highly flexible GMR-based microfluidic analytic devices have been demonstrated to analyze droplets of various dimensions and concentrations of magnetic contents.
24x10mm (300 x 300 DPI)

Cite this: DOI: 10.1039/c0xx00000x

www.rsc.org/xxxxxx

ARTICLE TYPE

Highly flexible and compact magnetoresistive analytic devices

Gungun Lin,*[a] Denys Makarov,*[a] Michael Melzer,[a] Wenping Si,[a,b] Chenglin Yan,[a,c] and Oliver G. Schmidt[a,b]

Received (in XXX, XXX) Xth XXXXXXXXX 20XX, Accepted Xth XXXXXXXXX 20XX

DOI: 10.1039/b000000x

A grand vision of realization of smart and compact multifunctional microfluidic devices for wearable health monitoring, environment sensing and point of care tests emerged with the fast development of flexible electronics. As a vital component towards this vision, magnetic functionality in flexible fluidics is still missing though demanded by the broad utility of magnetic nanoparticles in medicine and biology. Here, we demonstrate the first flexible microfluidic analytic devices with integrated high-performance giant magnetoresistive (GMR) sensors. Such devices can be bent to radius of 2 mm while still retaining its full performance. Various dimensions of magnetic emulsion droplets can be probed with high precision with limit of detection of 0.5 pl, providing broad applicability in high throughput droplet screening, flow cytometry and drug development. The flexible feature of the analytic devices holds great promise in the realization of wearable, implantable multifunctional platforms for biomedical, pharmaceutical and chemical applications.

Introduction

Flexible electronics represent a new generation of devices with exclusive features, for which conventional electronic devices relying on rigid substrates cannot surpass, i.e. reshaping its original form after fabrication, and even intimate contact with arbitrary geometries. Extensive research works have been reported on stretchable integrated circuits,[1,2] bendable batteries,[3,4] light emitting diodes,[5] flexible[6,7] and stretchable[8] magnetoelectronics, rollable electronic displays,[9,10] ultrathin transistors,[11,12] solar cells,[13] and paper-based electronics.[14] In recent years, technological developments have been driven from single functional element towards the realization of more complex integrated platforms. For instance, an active-matrix tactile sensing foil with arrays of integrated switching transistors and touch sensors was demonstrated.[11] Moreover, flexible electronics benefited from recent advances in microfluidics, leading to the emergence of a new type of flexible diagnostic devices or micro total analysis system (μTAS), which is cost efficient and suited for resource limited settings or poverty related conditions, and mechanically flexible appropriate for wearable, implantable biomedical devices or fluid delivery system. Flexible microfluidic devices have been reported on using label-free chemical sensing method on cellulose paper,[15-17] textiles[18] or polymeric substrates.[19]

Nonetheless, the diverse fields of microfluidics have seen extensive applications of magnetic nanoparticles in i.e., early detection or treatment of cancer,[20-22] immunological assays,[23] point-of-care tests,[24] and on-chip manipulations of biospecies.[25,26] Detection of magnetically-labelled biomarkers in complex biological samples with GMR[27-34], tunnelling magnetoresistance (TMR)[35,36] or hall sensors[37] have been realized on rigid platforms based on microarray format, which is capable of multiplex diagnostics or assays by detecting magnetic labels *statically* immobilized on substrates. However, the format is incapable of whole cell analyses. Recently, in-flow detection with magnetic sensors based on *cytometric* format addressed the need of analyses on cell level and promised high throughput enumerations of magnetically-labelled entities.[38-44] In addition, droplet-based microfluidics encapsulating biological species and magnetic nanoparticles can also benefit from the fast development of magnetic flow detection, as emulsion droplets armed with magnetic functionality can be used to transport, mix and release cargos in a controlled manner.[25,26] The effective on chip operations of emulsion droplets, however, relies on a clear identification of its volume and concentration of encapsulated magnetic nanoparticles. The evaluation of the as-synthesised magnetic micro-gels in droplet microfluidics primarily relied on optical observations,[45] while the instant feedback of which is crucial for process control. Thereby, accompanied by the eagerness and development of modern multifunctional biomedical devices which are light weight, inexpensive, wearable or even implantable, an inexpensive flexible integrated microfluidic platform combining both advantages from flexible electronics and fluidics, and possessing magnetic functionalities, i.e., for detection and quantification of magnetic objects in real time, is highly attractive and demanded.

Here, we fabricate the first highly flexible polymer-sandwiched giant magnetoresistive (GMR) device with integrated continuous microfluidic flow system, which processes magnetic functionality as demanded and is capable of probing magnetic objects encapsulated in emulsion droplets. The volume of droplets loaded with superparamagnetic nanoparticles ranges from hundreds of

picoliters to a few nanoliters, which can be well incorporated in lab-on-a-chip devices with low consumption volume while still providing sufficient amount of materials for on-chip manipulation. The detection limit for the magnetic content in an emulsion droplet of 1 nl was about 4 mg/ml, which is perfectly suited for full-range magnetic manipulations of droplets on chip including magnet disengagement, droplet dispersing and particle extraction.[26] The entire device can be bent down to radius of 2 mm still maintaining its full performance, which renders it the most flexible microfluidic analytic tool reported so far.

Materials and Methods

Preparation of substrates

A layer of SU-8 2 (MicroChem) photosensitive polymer was coated on a PET foil in order to reduce the surface roughness. TI-prime (MicroChem) was used as an adhesion promoter, before which a 5-min oxygen plasma treatment of 40 mW was performed to remove adsorbents. The spin coating speed of SU-8 2 was adjusted to 6000 rpm to produce a layer thickness about 800 nm. The spin coated SU-8 2 buffer was baked at 90°C on a hot plate for 5 min, and cross-linked by UV exposure using a Mask Aligner (Karl Suss, MJB4) followed by a post-bake at 90°C for 5 min.

Fabrication of GMR sensors

The sensor was prepared by magnetron sputtering technique. Before deposition, negative photoresist (AZ5214E, MicroChem) was spin coated on a PET foil buffered with SU-8 2 layer, which was subsequently patterned into a rectangular stripe with dimension of 6 μm × 100 μm by a standard photolithography technique using image reversal process. The deposition was performed under high vacuum condition with base pressure about 7.0×10^{-7} mbar. Ar was used as the sputter gas, the pressure of which was kept at 9.4×10^{-4} mbar. The structure of the sensor was revealed by lifting off the photoresist with acetone. After patterning the GMR sensors, a second step lithography based on lift-off process was used to pattern electrical contacts which were aligned with the sensors. Ta (5 nm)/Cu (200 nm)/Ta (5 nm) was used as the materials for the electrical contacts, which were deposited by magnetron sputtering technique.

Encapsulation of GMR sensors

In order to protect the GMR sensor from current leakage when it is integrated into a microfluidic channel, a SU-8 2 photosensitive polymer of thickness about 700 nm was spin coated on top of the sensor at spin speed of 8000 rpm. Afterwards, the SU-8 2 insulation layer was exposed under UV light with a mask aligner (MJB4, Karl Suss) to cross-link the polymers. After the exposure, the SU-8 2 layer was left without post-baking to retain epoxy groups in order to facilitate final assembly with a PDMS channel.

Assembly of the final device

The PDMS microfluidic channel was prepared based on a mould casting approach. Firstly, a layer of SU-8 50 (MicroChem) polymer was spin coated on a silicon wafer at the speed of 1000 rpm to obtain a layer thickness of 100 μm. Then the polymer was patterned by standard photolithography process, resulting in a channel width of 100 μm. A fresh PDMS (Silicone Elastomer KIT, Sylgard 184, Dow Corning) mixture (1:10 in wt%) was prepared and poured into the SU-8 50 mould and cured at 200° for 5 min. Afterwards, the cured PDMS channel was peeled off from the silicon wafer. The inlets/outlets of the channel were created through PDMS using a biopsy puncher with a diameter of 1 mm. The assembly of the device was finalized by bonding PDMS channel to the SU-8-encapsulated chip. A N_2 plasma treatment of 3 min and 40 mW was used to produce amine-terminated groups on PDMS surface.[53] Then the chip and the PDMS channel were brought into contact under an optical microscope to precisely align the channel with the sensors. Finally, the device was baked at 120°C on a hot plate for 30 min to achieve a permanent bonding between PDMS and the chip.

Experimental setup

Magnetoelectrical characterizations were performed with a four-probe geometry in a magnetoelectrical testing station. The GMR sensors were placed in between two pole shoes of the electromagnets, where magnetic fields could be swept between ±30 mT which was sufficient to saturate the sensor. The GMR sensor was powered by a constant current while the voltage change was recorded by a programmed multimeter (Keithley Model 2000). The bending experiments were realized on a motor-controlled mechanical loading setup. The sample was mounted on a loading stage, one end of which was precisely driven by a motor to move over a defined distance while the other end was fixed. Meanwhile, the stage was placed inside the above mentioned magnetoelectrical testing station, from which GMR curves could be measured on samples in different bending states.

For the real time detection of emulsion droplets, a measurement setup was established based on a Wheatstone bridge (see details in ESI†). The whole bridge was powered by a lock-in amplifier, the differential voltage signal ΔV of which was fed in to the lock-in to improve the signal to noise ratio. The analogue output from the lock-in was picked up by an analogue/digital converter (NI-USB 6800, National Instrument). A constant AC measuring current of 1 mA was used. An internal lock-in sinusoidal signal with a frequency of 1 kHz and amplitude of 0.08 V was used as a reference. The sampling rate of the AD converter is 5 kHz. The measurement range of the lock-in was 500 μV. For the measurement, an external permanent magnet is placed below the sensor. As the sensor is sensitive to the in-plane magnetic field, the in-plane component of the stray fields from the magnet is used to bias the sensor to the most sensitive region. The position of the magnet was carefully adjusted via monitoring the sensor output and fixed during the whole measurement of droplets.

Utilized reagents

The substrate used is a transparent, flexible sheet of PET with thickness of 100 μm. To produce stable magnetic droplets in a microfluidic channel, hydrocarbon oil (Vacuum pump fluid, TKO 19 Ultra, Kurt J. Lesker) mixed with 5 wt% of SPAN 80 was used as the continuous phase and magnetic nanoparticles (Ferrotec, EMG 700) diluted with different amount of DI water was used as the disperse phase.

Results and Discussions

Fabrication of flexible magnetoresistive analytic devices

For probing of magnetic particles or emulsion droplets in microfluidics, a magnetic sensor with high sensitivity and small effective sensing area which is comparable to the dimension of objects to be detected is required.[46] The signal is essentially related to the effective magnetic stray fields of the magnetic entities that could be detected by a magnetic sensor.[42,46] To fulfill the stringent requirements on the sensor sensitivity, high-performance sensing elements relying on GMR effect should be applied. In this respect, GMR multilayers and spin valve sensors were already successfully fabricated on flexible[6,7] as well as elastic membranes.[48,49] In the present work, we chose highly sensitive GMR [Py(1.5 nm)/Cu(2.3 nm)]$_{30}$ multilayers (Py=$Ni_{81}Fe_{19}$) coupled at the 2nd antiferromagnetic maximum prepared on a transparent, flexible sheet of polyethylene terephthalate (PET). The thickness of PET is 100 µm, which is mechanically stable to sustain high pressure during continuous pumping in a microfluidic channel while still maintaining the advantage for the device of getting reshaped as needed. The fabrication process of a flexible microfluidic magnetic device based on a polymer-sandwiched GMR sensor is displayed in Figure 1. A strong advantage of the platform on a flexible foil over conventional electronics integrated in microfluidic channels fabricated on silicon or glass substrates is the possibility of fabrication over large areas (Fig. 1b) and redesigning the substrate at will. For instance, a single working unit can be cut out of a flexible foil (Supplementary Movie), or redundant parts of the support for specific applications can be removed simply by cutting.

As a first step, we used flexible SU-8 polymeric material to buffer the GMR sensor, as the commercially available PET foil used is characterized with a relatively pronounced roughness (~15 nm, root mean square) which can affect the interfacial mediated GMR effect.[50] Coating SU-8 on a PET foil flattens its surface substantially (Fig. S2). Magnetoelectrical characterizations of [Py/Cu]$_{30}$ multilayers coupled at the 1st and 2nd antiferromagnetic maximum deposited on different supports (PET foil, polymer-buffered PET foil and silicon substrate) are compared in Fig. S1. The enhancement of the GMR ratio after polymer-buffering is attributed to the enhancement of the interlayer exchange coupling strength at reduced roughness.[50]

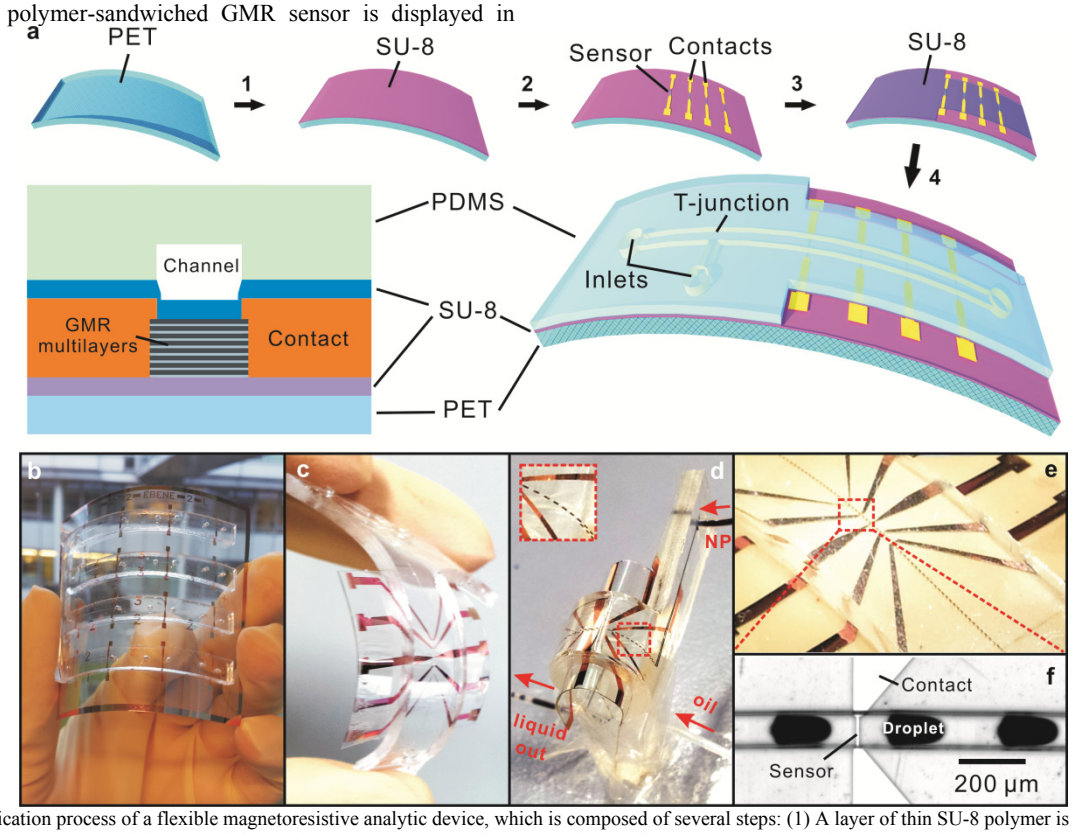

Fig. 1 (a) Fabrication process of a flexible magnetoresistive analytic device, which is composed of several steps: (1) A layer of thin SU-8 polymer is spin coated on a flexible PET foil. (2) GMR multilayers and electrical contacts are patterned on a SU-8 buffered PET foil. (3) A second thin SU-8 polymer is coated on top of sensors and contacts as an insulating layer. (4) PDMS-casted microfluidic channel is assembled with bottom polymer-sandwiched GMR sensors. (Bottom left in Panel-a) Schematic representation of the cross-section of a flexible polymer-sandwiched microfluidic GMR device. (b) Photograph of a large area of electrodes integrated with microfluidic channels. (c) Photograph of a flexible GMR-based analytical device. (d) Photograph of a highly flexible GMR-based analytic device filled with liquid and producing emulsion droplets on chip. (Inset) Magnification of the part marked with a red rectangle on the chip. (e) The real time detection of a train of emulsion droplets with encapsulated magnetic nanoparticles (f) which are passing across the sensor.

To ensure highest sensitivity, it is crucial to adjust the size of the GMR sensor to be compatible to the dimension of the magnetic objects under investigation. A top-down approach was used to structure the GMR sensors into rectangular stripes with a constant width of 6 µm and different length of 20, 40, 60, and 100 µm (Fig. S5). Detailed characterizations of the structured GMR sensors reveal that the change of the sensor resistance scales with the aspect ratio of GMR sensors. Independent of the length, the performance of the sensors patterned on one substrate remains the same with GMR ratio of about 14%. The variability of the

sensitivity of these patterned sensors on one substrate is ± 0.05%/Oe. The GMR ratio is defined as the magnetic field, H_{ext}, dependent change of sample resistance: $GMR(H_{ext}) = (R(H_{ext}) - R(H_{sat})) / R(H_{sat})$, where $R(H_{sat})$ is the sensor resistance when saturating magnetic field, H_{sat}, is applied.[48] A GMR sensor (width 6 µm × length 100 µm, Fig. 2b, upper panel) was integrated in a microfluidic channel with a cross-section area of 100 × 100 $µm^2$ (Fig. 2b, bottom panel). The magneto-electrical characterization of the integrated sensor (Fig. 2a) confirms the excellent performance of the device with a GMR ratio of 14% and maximum sensitivity of 0.4%•Oe^{-1} at low field of 12 Oe. Here the sensitivity is given by: $S(H_{ext}) = [dR(H_{ext})/dH_{ext}]/R(H_{sat})$.[48] With the variability of the sensitivity of GMR sensors between substrates being within ± 0.1%/Oe, the performance of the polymer-buffered GMR sensor on PET foil is higher than the one (0.26%/Oe) previously demonstrated on a silicon substrate,[41] which could be ascribed to the enhanced interlayer exchange coupling across GMR multilayers as described in previous work.[50]

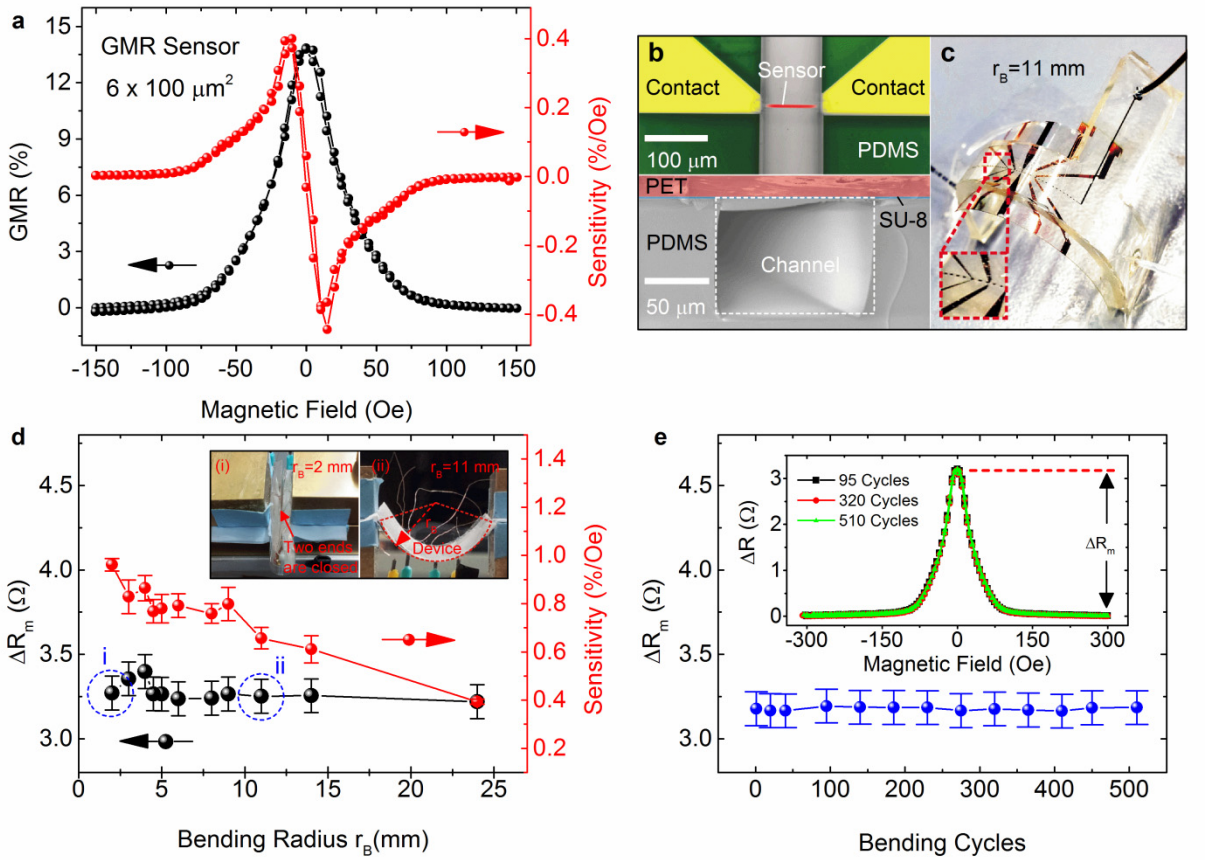

Fig. 2 (a) GMR curve (black) and derived magnetic field dependent sensitivity (red) of a flexible GMR sensor stripe with size of 6 x 100 µm². (b) (Upper panel) Color-coded micrograph of a flexible GMR sensor stripe integrated into a PDMS microfluidic channel. (Bottom panel) SEM image of the cross-section of the microfluidic channel cut by a scissor. The channel has a height and width of 100 µm each. (c) Photographs of the device filled with liquid and producing emulsion droplets with encapsulated magnetic nanoparticles (NP) with bending radius of 11 mm. Inset is magnification of the part marked with red rectangle. The small black dots visible in the channel are emulsion droplets as-produced in the microfluidic channel. (d) Response of the GMR device at different bending states. The maximum change of the resistance (ΔR_m, see inset in (e)) of the GMR sensor was recorded for different bending radii. The maximum average sensitivity of the sensor is plotted against different bending radii (red). The insets show photographs of the device which is bent to a bending radius (r_B) of: 2 mm (i), when two ends of the device were closed, and 11 mm (ii). Error bars of the maximum sensitivity are standard deviations of the 4 sensitivity values derived during one cycle of magneto-electrical characterization. (e) The maximum change of the sensor resistance during cyclic bending. For the experiment, the device was reversibly bent from the relaxed state to radius of 8 mm. The inset shows the change of the sensor resistance for a magnetic field sweep after 95, 320, and 510 cycles of bending and unbending. Error bars for ΔR_m in (d) and (e) are the precision of a multimeter (Keithley 2000) used for measuring the resistance.

To ensure the operation of the GMR sensor in liquid environments, an appropriate electrical insulation is required. We went beyond the traditional insulating approach, i.e., covering with a layer of brittle oxides, such as SiO_2 and Al_2O_3.[42] Instead, we adopted a strategy by encapsulating the sensor between two flexible polymer layers. As SU-8 is an epoxy-based polymer, the whole assembly process with the PDMS channel is facilitated by creating amine groups on the PDMS surface and harnessing the epoxy-amine reaction (details on preparation are given in the methods section).[53] The assembly process was carried out without liquid condition for which usually drying out the whole device was tedious and time consuming. The final assembled device is shown in Fig. 1c. The fluidic functionality is demonstrated by its capability of delivering fluids and producing emulsion droplets on chip (Fig. 1d-1f).

Mechanical performance of the device

The whole GMR device (integrated sensor size: 6×100 µm²) with an integrated microfluidic channel was mounted on a mechanical loading stage, on which the device could be continuously bent and corresponding magnetoelectrical characterizations of the GMR sensor were simultaneously performed. Fig. 2d-2e shows the performance of the integrated GMR sensor during bending tests. The total thickness of the device including the PDMS

channel is about 2.3 mm. We continuously bent the device until two of its ends were almost closed (Fig. 2d, inset-i), revealing a minimum bending radius of about 2 mm which is superior to conventional inorganic materials of 100 µm thickness that can only reach a bending limit of about 5 mm.[51] The total electrical resistance (including the sensor and electrical contacts) was measured without applying an external magnetic field and at an external magnetic field of 300 Oe (Fig. S6d), respectively, when the device was gradually bent to the minimum radius of 2 mm. The consistent behavior of the measured total resistance shows that the sensor was well electrically contacted during the entire bending cycle. A slight reduction of the saturation field of the sensor can be observed from the measurement of the resistance change under cyclic magnetic fields (Fig S6c) possibly due to magnetostriction effect, however, the sensor is still functional without degrading the performance, which is reflected by the constant maximum change of sensor resistance R_m with magnetic field during the magneto-electrical characterizations (Fig. 2d). For the magnetic detection, the reduction of the saturation field leads to the corresponding reduction of the sensing range for magnetic in-flow detection. However, the sensitivity of the sensor increases from about 0.4%/Oe to about 1%/Oe with increasing bending of the device.

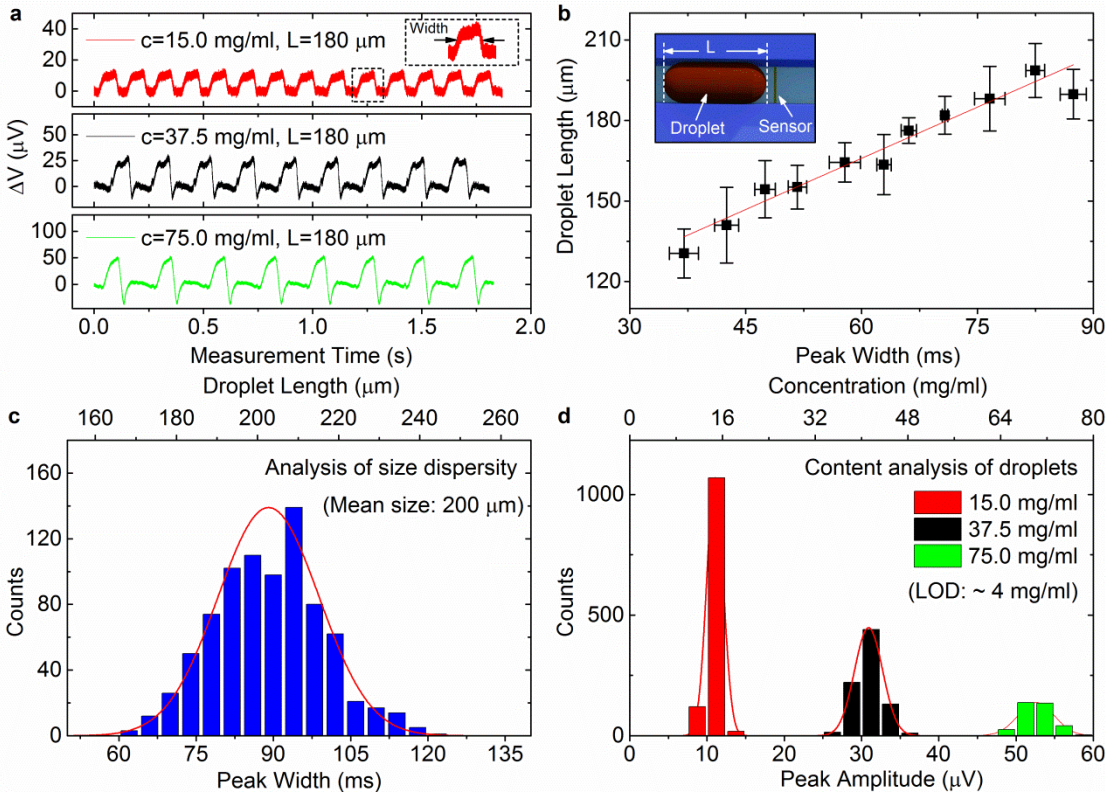

Fig. 3 (a) Real time in-flow detection of magnetic droplets of different concentrations, c, of encapsulated magnetic nanoparticles for a train of droplets with size of 180 µm (within 2 s of measurement time). The voltage change (ΔV) of the device is recorded over time. (b) Dependence of the measured droplet length on the detection peak width for sequentially produced droplets of various sizes. The line represents a linear fit of the data. (Inset) Schematic sketch of a droplet in a microfluidic channel with the droplet length (denoted by L) measured along the travelling direction. (c) Histograms of the detection peak width for around 1000 emulsion droplets containing magnetic nanoparticles of 37.5 mg/ml. Top x-axis denotes the corresponding droplet length. The red curve shows a Gaussian fit to the histogram. (d) Histograms of the detection peak amplitude for more than 1000 emulsion droplets of different concentrations of encapsulated magnetic nanoparticles (15.0 mg/ml, 37.5 mg/ml and 75.0 mg/ml). Top x-axis corresponds to the concentration of encapsulated magnetic nanoparticles. The curves show Gaussian fits to the respective histograms.

The robustness of the device against uninterrupted mechanical deformation was tested by reversibly bending the same device back and forth to a target radius of 8 mm. Remarkably, more than 500 cycles of bending were achieved with the device delivering full performance without any detachment of the microfluidic channel from the substrate. Also the sensor and electrical contacts did not show any degradation in performance in terms of the measured total resistance (Fig. S6e) and the maximum change of the sensor resistance during magnetoelectrical characterizations (Fig. 2e), which is reflected in exact overlapping of the measured GMR curves summarizing the change of the sensor resistance with varying magnetic fields after different bending cycles (Fig. 2e, inset). One of the primary goals of fabricating an effective flexible microfluidic device is to demonstrate its capability of delivering liquids under various bending states. We connected the device to external supply tubes where hydrocarbon oil and aqueous magnetic nanoparticles can be injected via two separate inlets. Various bended states were realized by gradually closing the two ends of the device which were fixed on a stage (Fig. 2c & Fig. S7). It is clearly visible that magnetic emulsion droplets can be well produced even when the device was bent to the minimum radius of 2 mm (Fig. 1d), thus demonstrating to be the most flexible microfluidic device reported so far.

Analytic features of the device

To demonstrate the magnetic functionality of the device, superparamagnetic ferrofluid nanoparticles with nominal particle size of 10 nm (Ferrotec, EMG 700) were encapsulated inside the

emulsion droplets formed by a T-shape on-chip junction (Fig. S4). The emulsion droplets were pumped across the surface of an integrated GMR sensor one by one. As the ferrofluid magnetic nanoparticles are superparamagnetic, an external permanent magnet made of AlNiCo (A1045, IBSMagnet) was placed below the sensor to induce the net magnetic moment from the droplets and simultaneously bias the sensor to the most sensitive region (Details are provided in ESI†). The magnetic stray fields of the ferrofluid emulsion droplets were detected by the integrated GMR sensor, which is evidenced by characteristic detection events of the droplets consisting of isolated peaks of the voltage signal (Fig. 3a). The detection peak features its signal width and amplitude. As a GMR sensor is a proximity sensor, only local magnetic stray fields contribute to the final detected signal. Owing to this feature, the dimension of an emulsion droplet containing magnetic nanoparticles can be derived from the detection peak width. Further, as the amplitude of magnetic stray fields is proportional to the amount of magnetic nanoparticles in a droplet, the amplitude of the detection signal is related to the amount of magnetic content in the droplets, rendering the device an analytical tool.[41]

The real time in-flow detection of magnetic droplets of different concentrations of encapsulated magnetic nanoparticles is shown in Figure 3a. The detection peak features a local maximum and a local minimum in signal amplitude located at the rising and falling edge, respectively, as local stray field maximum and minimum occur at the two ends of a magnetic droplet when it is magnetized by an external magnetic field.[41] Fig. 3a shows that the detection of emulsion droplets of the same size but loaded with more concentrations of magnetic nanoparticles gives higher signal amplitudes (~ 55 μV for 75 mg/ml, ~ 30 μV for 37.5 mg/ml and ~ 10 μV for 15.0 mg/ml of magnetic nanoparticles). We further produced a train of magnetic emulsion droplets of various sizes. As the detection peak width is independent of the concentration of magnetic nanoparticles in a droplet, it can be used to correlate the individual detection peak with each passing emulsion droplet.[41] The real time detection of these emulsion droplets is displayed in Fig. S8. Fig. 3b plots the measured droplet size (denoted by L in schematic sketch) against the detection peak width for the sequentially produced droplets. We observe a clear linear dependence of the droplet size on the peak width. The coefficient (1.3±0.1 mm/s) between the droplet size and the peak width derived by a linear fit of the data agrees well with the flowing speed of the droplets (1.5±0.1 mm/s, determined by video analysis) in the microfluidic channel. The slight deviation from a perfect linear relationship is caused by the deviation in measuring the droplet length and the peak width, which is because of the limited resolution (10 μm) of optical digital microscope (ISM-PM160 L) and the slight deviation (± 0.1 mm/s) of the flow speed. The precision of the detection peak width (1 ms) obtained with the device is determined by electronic settings (sampling rate of 5 kHz), which reveals that the precision of determining the droplet size is about 1.5 μm under the constant flow speed of 1.5 mm/s. Thus, the magnetic sensors provide very precise information on the size of emulsion droplets without use of complex and bulky optical detection schemes,[52] which is crucial for applications in wearable diagnostic electronics.

Furthermore, the device allows monitoring the evolution of droplets under various flow mechanisms, i.e. distinguishing between squeezing and dripping regimes in microfluidics without use of optical methods. We put forth a theoretical model (Fig. S9), which allows correlating the reduction of the droplet volume to the decrease of the amplitude and width of detection peaks when the droplet is smaller than the channel dimension. The minimum size of an emulsion droplet encapsulated with 37.5 mg/ml of magnetic nanoparticles that can be detected by the device is estimated to be 10 μm in diameter (~ 0.5 pl in volume) in a channel with a cross-section area of 100 x 100 μm^2, which unveils the potential of the device in applications such as sensing magnetic objects encapsulated in even much smaller volume, i.e., magnetically-labeled biological cells for cytometry applications.

As the device is capable of resolving magnetic emulsion droplets in terms of size and magnetic content, it can find its application in analyzing the distribution of droplet size and concentration of magnetic nanoparticles over large arrays. For example, histograms of the peak width (Fig. 3c) and amplitude (Fig. 3d) are used to statistically analyze the distribution of size and concentrations of magnetic nanoparticles in a large scale of emulsion droplets, respectively. A Gaussian fit to the histogram reveals that the average size of around 1000 as-produced droplets is about 200 μm with a standard deviation of 12 μm; while Fig. 3d analyzes the magnetic content of more than 1000 droplets encapsulating different concentrations of loaded magnetic nanoparticles. We measured emulsion droplets of around 1 nl containing various concentrations of magnetic nanoparticles ranging from 15.0 mg/ml to 75 mg/ml, the voltage signal on different concentrations of magnetic nanoparticles is shown in Fig. S10. Linear interpolation of the data to the noise level of the device (~ 2.5 μV) reveals the limit of detection (LOD) of the device of around 4 mg/ml, enabling the device as a quantification tool for the identification of the amount of magnetic materials used for on-chip manipulation of emulsion droplets encapsulated with other reagents.[25]

The current LOD of the device is set by several factors, i.e. the thickness of the insulation layer, the magnetic field configuration used for biasing the sensor and magnetizing nanoparticles, as well as measurement electronics. A detailed comparison of the present device with prior works on the LOD has been made in ESI†. As shown, the LOD of the magnetic moment of a droplet for the present device is about 2 x 10^{-10} emu for a droplet of 0.5 pl, which is estimated for a microfluidic channel with a height of 100 μm. The LOD of our device is comparable with previously reported value (2 x 10^{-10} emu) with devices integrated in a 10 μm high channel.[55] Thus, a hydrodynamic focusing approach[39] could be used to reduce the physical separation distance between the sensor and targets to detect such small droplets (0.5 pl), or bacteria and pathogens with even smaller dimension (~ 1 μm). Further, the thickness of the insulation layer (~ 700 nm) could be further reduced to enhance sensitivity as the signal level inversely scales with z^3 (z being the distance of magnetic objects from the sensor surface). In addition, relatively larger out-of-plane magnetic field (up to 190 mT) can be used to induce larger magnetic moment of magnetic nanoparticles to magnetize without saturating the sensor.[42]

Conclusions

In summary, we developed a flexible microfluidic device equipped with in-situ magnetic functionality. Compared with present existing magnetic flow detectors fabricated on rigid substrates,[40-44] the direct advantages our approach provides are the feasibility of cost-efficient production and perspectives of mass production due to the low cost and light weight of flexible foils. The remarkable mechanical properties of the device compared with rigid counterparts, i.e., minimum bending radius of 2 mm and over 500 cycles of bending, also promises the long term stability of the device for practical applications.

Although the current device possesses merely magnetic functionality, it could be extended for future applications. An example can be made in the application of *in vivo* flow cytometry, which is performed directly in the human body. In such a case, magnetic nanoparticles have been used to enrich biomarkers to the near-skin area to enhance the detection which combines already optical and acoustical methods.[54] Naturally, a magnetic functional element could be used for such application to directly detect biomarkers labeled with magnetic particles. In order to have the best compliance to the human body, a bendable device which can provide such magnetic functionality is anticipated. Our present device provides the state-of-the-art solution to incorporate magnetic elements on a flexible platform that could be potentially implemented in such kind of modern biomedical devices by combining optical, magnetic, acoustical, and chemical sensitivities in order to realize modern multifunctional biomedical devices which are light weight, wearable or even implantable.

Notes and references

[a] *Institute for Integrative Nanosciences, IFW Dresden, Helmholtzstr. 20, 01069 Dresden, Germany; E-mail: g.lin@ifw-dresden.de, d.makarov@ifw-dresden.de*
[b] *Material Systems for Nanoelectronics, Chemnitz University of Technology, Reichenhainerstr. 70, 09107 Chemnitz, Germany;*
[c] *School of Energy, Soochow University, 215006 Suzhou, Jiangsu, People's Republic of China;*

† Electronic Supplementary Information (ESI) available: [details of any supplementary information available should be included here]. See DOI: 10.1039/b000000x/

‡ Footnotes should appear here. These might include comments relevant to but not central to the matter under discussion, limited experimental and spectral data, and crystallographic data.

1 D.-H. Kim, J.-H. Ahn, W. M. Choi, H.-S. Kim, T.-H. Kim, J. Song, Y. Y. Huang, Z. Liu, C. Lu, J. A. Rogers, Science 2008, 320, 507.
2 J. A. Rogers, T. Someya, Y. Huang, Science 2010, 327, 1603–7.
3 H. Nishide, K. Oyaizu, Science 2008, 319, 737–8.
4 N. Li, Z. Chen, W. Ren, F. Li, H.-M. Cheng, Proc. Natl. Acad. Sci. U. S. A. 2012, 109, 17360–5.
5 M. S. White, M. Kaltenbrunner, E. D. Głowacki, K. Gutnichenko, G. Kettlgruber, I. Graz, S. Aazou, C. Ulbricht, D. A. M. Egbe, M. C. Miron, Z. Major, M. C. Scharber, T. Sekitani, T. Someya, S. Bauer, N. S. Sariciftci, Nat. Photonics 2013, 7, 811–816..
6 S. S. P. Parkin, Appl. Phys. Lett. 1996, 69, 3092.
7 Y. Chen, Y. Mei, R. Kaltofen, J. I. Mönch, J. Schumann, J. Freudenberger, H.-J. Klauß, O. G. Schmidt, Adv. Mater. 2008, 20, 3224–3228.
8 M. Melzer, D. Makarov, A. Calvimontes, D. Karnaushenko, S. Baunack, R. Kaltofen, Y. Mei, O. G. Schmidt, Nano Lett. 2011, 11, 2522–6.
9 G. H. Gelinck, H. E. A. Huitema, E. van Veenendaal, E. Cantatore, L. Schrijnemakers, J. B. P. H. van der Putten, T. C. T. Geuns, M. Beenhakkers, J. B. Giesbers, B.-H. Huisman, E. J. Meijer, E. M. Benito, F. J. Touwslager, A. W. Marsman, B. J. E. van Rens, D. M. de Leeuw, Nat. Mater. 2004, 3, 106–10.
10 Y. Chen, J. Au, P. Kazlas, A. Ritenour, H. Gates, M. McCreary, Nature 2003, 423, 136.
11 M. Kaltenbrunner, T. Sekitani, J. Reeder, T. Yokota, K. Kuribara, T. Tokuhara, M. Drack, R. Schwödiauer, I. Graz, S. Bauer-Gogonea, S. Bauer, T. Someya, Nature 2013, 499, 458–63.
12 G. A. Salvatore, N. Münzenrieder, T. Kinkeldei, L. Petti, C. Zysset, I. Strebel, L. Büthe, G. Tröster, Nat. Commun. 2014, 5, 2982.
13 M. Kaltenbrunner, M. S. White, E. D. Głowacki, T. Sekitani, T. Someya, N. S. Sariciftci, S. Bauer, Nat. Commun. 2012, 3, 770.
14 F. Eder, H. Klauk, M. Halik, U. Zschieschang, G. Schmid, C. Dehm, Appl. Phys. Lett. 2004, 84, 2673.
15 W. Dungchai, O. Chailapakul, C. S. Henry, Anal. Chem. 2009, 81, 5821–6.
16 Z. Nie, C. A. Nijhuis, J. Gong, X. Chen, A. Kumachev, A. W. Martinez, M. Narovlyansky, G. M. Whitesides, Lab Chip 2010, 10, 477–83.
17 . N. Godino, R. Gorkin, K. Bourke, J. Ducrée, Lab Chip 2012, 12, 3281–4.
18 F. Vatansever, R. Burtovyy, B. Zdyrko, K. Ramaratnam, T. Andrukh, S. Minko, J. R. Owens, K. G. Kornev, I. Luzinov, ACS Appl. Mater. Interfaces 2012, 4, 4541–8.
19 S. Metz, A. Bertsch, D. Bertrand, P. Renaud, Biosens. Bioelectron. 2004, 19, 1309–1318.
20 E. I. Galanzha, E. V Shashkov, T. Kelly, J.-W. Kim, L. Yang, and V. P. Zharov, *Nat. Nanotechnol.*, 2009, **4**, 855–60.
21 L. C. Branquinho, M. S. Carrião, A. S. Costa, N. Zufelato, M. H. Sousa, R. Miotto, R. Ivkov, A. F. Bakuzis, Sci. Rep. 2013, 3, 2887.
22 S. J. Osterfeld, H. Yu, R. S. Gaster, S. Caramuta, L. Xu, S.-J. Han, D. A. Hall, R. J. Wilson, S. Sun, R. L. White, R. W. Davis, N. Pourmand, S. X. Wang, Proc. Natl. Acad. Sci. U. S. A. 2008, 105, 20637–40
23 L. A. Sasso, I. H. Johnston, M. Zheng, R. K. Gupte, A. Ündar, J. D. Zahn, Microfluid. Nanofluidics 2012, 13, 603–612.
24 R. S. Gaster, D. A. Hall, S. X. Wang, Lab Chip 2011, 11, 950–6.
25 J. S. Sander, R. M. Erb, C. Denier, A. R. Studart, Adv. Mater. 2012, 24, 2582–7, 2510.
26 Y. Zhang, T.-H. Wang, Adv. Mater. 2013, DOI 10.1002/adma.201300383.
27 R. S. Gaster, D. A. Hall, C. H. Nielsen, S. J. Osterfeld, H. Yu, K. E. Mach, R. J. Wilson, B. Murmann, J. C. Liao, S. S. Gambhir, and S. X. Wang, *Nat. Med.*, 2009, **15**, 1327–32.
28 V. C. Martins, F. A. Cardoso, J. Germano, S. Cardoso, L. Sousa, M. Piedade, P. P. Freitas, and L. P. Fonseca, *Biosens. Bioelectron.*, 2009, **24**, 2690–5.
29 G. Reiss, H. Brueckl, A. Huetten, J. Schotter, M. Brzeska, M. Panhorst, D. Sudfeld, A. Becker, P. B. Kamp, A. Puehler, K. Wojczykowski, and P. Jutzi, *J. Mater. Res.*, 2011, **20**, 3294–3302.
30 J. C. Rife, M. M. Miller, P. E. Sheehan, C. R. Tamanaha, M. Tondra, and L. J. Whitman, *Sensors Actuators A Phys.*, 2003, **107**, 209–218.
31 X. Zhi, Q. Liu, X. Zhang, Y. Zhang, J. Feng, and D. Cui, Lab Chip, 2012, 12, 741–5.
32 X. Zhi, M. Deng , H. Yang, G. Gao, K. Wang, H. Fu, Y. Zhang, D. Chen, D. Cui, Biosens. Bioelectron., 2014; 54, 372–377.
33 R. L. Millen, J. Nordling, H. A. Bullen, M. D. Porter, M. Tondra, M. C. Granger. *Anal Chem*., 2008, 80, 7940–7946.
34 R. L. Millen, T. Kawaguchi, M. C. Granger, M. D. Porter, M. Tondra. Anal Chem. 2005, 77, 6581–6587.

Acknowledgements

The authors thank Dr. L. Baraban (TU Dresden) for fruitful discussions on magnetic cytometry, I. Fiering (IFW Dresden) for assistance in metal deposition, B. Eichler for AFM measurements. We acknowledge the financial support from the DFG Research Group 1713 and European Research Council under the European Union's Seventh Framework Programme (FP7/2007-2013)/ERC grant agreement n° 306277.

35 W. Shen, B. D. Schrag, M. J. Carter, and G. Xiao, *Appl. Phys. Lett.*, 2008, **93**, 33903.

36 F. A. Cardoso, J. Germano, R. Ferreira, S. Cardoso, V. C. Martins, P. P. Freitas, M. S. Piedade, and L. Sousa, *J. Appl. Phys.*, 2008, **103**, 07A310.

37 S. Gambini, K. Skucha, P. P. Liu, J. Kim, and R. Krigel, IEEE J. Solid-State Circuits, 2013, 48, 302–317.

38 D. Issadore, J. Chung, H. Shao, M. Liong, A. A. Ghazani, C. M. Castro, R. Weissleder, and H. Lee, *Sci. Transl. Med.*, 2012, **4**, 141ra92.

39 D. Issadore, H. J. Chung, J. Chung, G. Budin, R. Weissleder, and H. Lee, *Adv. Healthc. Mater.*, 2013, **2**, 1224–8.

40 I. Mönch, D. Makarov, R. Koseva, L. Baraban, D. Karnaushenko, C. Kaiser, K.-F. Arndt, and O. G. Schmidt, *ACS Nano*, 2011, **5**, 7436–42.

41 G. Lin, L. Baraban, L. Han, D. Karnaushenko, D. Makarov, G. Cuniberti, O. G. Schmidt, Sci. Rep. 2013, 3, 2548.

42 J. Loureiro, P. Z. Andrade, S. Cardoso, C. L. da Silva, J. M. Cabral, P. P. Freitas, Lab Chip 2011, 11, 2255–61.

43 K. Aledealat, G. Mihajlovic, K. Chen, M. Field, G. J. Sullivan, P. Xiong, P. B. Chase, and S. von Molnar, *J. Magn. Magn. Mater.*, 2010, **322**, L69–L72.

44 N. Pekas, M. D. Porter, M. Tondra, A. Popple, and A. Jander, *Appl. Phys. Lett.*, 2004, **85**, 4783.

45 C.-H. Chen, A. R. Abate, D. Lee, E. M. Terentjev, D. A. Weitz, Adv. Mater. 2009, 21, 3201–3204.

46 M. Tondra, M. Porter, R. J. Lipert, J. Vac. Sci. Technol. A-vacuum Surfaces Film. 2000, 18, 1125–1129.

47 S. S. P. Parkin, K. P. Roche, T. Suzuki, Jpn. J. Appl. Phys. 1992, 31, L1246–L1249

48 M. Melzer, D. Karnaushenko, D. Makarov, L. Baraban, A. Calvimontes, I. Mönch, R. Kaltofen, Y. Mei, O. G. Schmidt, RSC Adv. 2012, 2, 2284.

49 M. Melzer, G. Lin, D. Makarov, O. G. Schmidt, Adv. Mater. 2012, 24, 6468–72.

50 Y. Chen, Y. Mei, A. Malachias, J. Ingolf Mönch, R. Kaltofen, O. G. Schmidt, J. Phys. Condens. Matter 2008, 20, 452202

51 T. Someya, Stretchable electronics, John Wiley & Sons, (2012).

52 L. Baraban, F. Bertholle, M. L. M. Salverda, N. Bremond, P. Panizza, J. Baudry, J. A. G. M. de Visser, and J. Bibette, *Lab Chip*, 2011, **11**, 4057–62.

53 Z. Zhang, P. Zhao, G. Xiao, B. R. Watts, and C. Xu, *Biomicrofluidics*, 2011, **5**, 46503–465038.

54 E. I. Galanzha, E. V Shashkov, T. Kelly, J.-W. Kim, L. Yang, and V. P. Zharov, *Nat. Nanotechnol.*, 2009, **4**, 855–60.

55 I. Jeong, et al., Journal of Magnetics, 2012, 17, 4, 302.